Published online 15 October 2016 *Nucleic Acids Research, 2016, Vol. 44, No. 20* ***10003–10014***
doi: 10.1093/nar/gkw930

Engineering of temperature- and light-switchable Cas9 variants

Florian Richter[1,*], Ines Fonfara[2,3], Boris Bouazza[1], Charlotte Helene Schumacher[1], Majda Bratovič[2], Emmanuelle Charpentier[2,3] and Andreas Möglich[1,4,*]

[1]Biophysikalische Chemie, Institut für Biologie, Humboldt-Universität zu Berlin, 10115 Berlin, Germany, [2]Max-Planck-Institute for Infection Biology, 10117 Berlin, Germany, [3]The Laboratory for Molecular Infection Medicine Sweden (MIMS), Umeå Centre for Microbial Research (UCMR), Department of Molecular Biology, Umeå University, Umeå 90187, Sweden and [4]Lehrstuhl für Biochemie, Universität Bayreuth, 95447 Bayreuth, Germany

Received July 25, 2016; Revised October 05, 2016; Accepted October 06, 2016

ABSTRACT

Sensory photoreceptors have enabled non-invasive and spatiotemporal control of numerous biological processes. Photoreceptor engineering has expanded the repertoire beyond natural receptors, but to date no generally applicable strategy exists towards constructing light-regulated protein actuators of arbitrary function. We hence explored whether the homodimeric *Rhodobacter sphaeroides* light-oxygen-voltage (LOV) domain (*Rs*LOV) that dissociates upon blue-light exposure can confer light sensitivity onto effector proteins, via a mechanism of light-induced functional site release. We chose the RNA-guided programmable DNA endonuclease Cas9 as proof-of-principle effector, and constructed a comprehensive library of *Rs*LOV inserted throughout the Cas9 protein. Screening with a high-throughput assay based on transcriptional repression in *Escherichia coli* yielded paRC9, a moderately light-activatable variant. As domain insertion can lead to protein destabilization, we also screened the library for temperature-sensitive variants and isolated tsRC9, a variant with robust activity at 29°C but negligible activity at 37°C. Biochemical assays confirmed temperature-dependent DNA cleavage and binding for tsRC9, but indicated that the light sensitivity of paRC9 is specific to the cellular setting. Using tsRC9, the first temperature-sensitive Cas9 variant, we demonstrate temperature-dependent transcriptional control over ectopic and endogenous genetic loci. Taken together, *Rs*LOV can confer light sensitivity onto an unrelated effector; unexpectedly, the same LOV domain can also impart strong temperature sensitivity.

INTRODUCTION

Sensory photoreceptors are the biological agents that mediate light sensation in manifold organisms. Photoreceptors comprise photosensor modules which absorb incident light and effector modules which possess biological activity and elicit downstream physiological adaptations (1). This modular, genetically encodable architecture lends itself to the engineering of novel photoreceptors via recombination of photosensors and effectors (2). Engineered photoreceptors not only serve as light-regulated actuators in optogenetics, but also provide mechanistic insight into principles of signal transduction. The two most versatile and successful photoreceptor engineering strategies to date (2) rely on light-regulated order-disorder transitions (3) and light-regulated association reactions (4), respectively. Although numerous effector activities have thus been subjected under light control, no generally applicable route towards creating photoactivatable variants of arbitrary effectors yet exists, especially in case the effector is monomeric and no natural regulatory mechanism is known (2). To expand the repertoire of available strategies, we set out to explore the potential of the photoreceptor *Rs*LOV (5) (Figure 1a) from *Rhodobacter sphaeroides* for the engineering of light-regulated protein actuators. *Rs*LOV belongs to the family of light-oxygen-voltage (LOV) photoreceptors (6) that employ flavin nucleotide chromophores to respond to blue light. In its dark-adapted form, *Rs*LOV predominantly assumes homodimeric state with the dimer interface formed by ancillary helices N-terminal (A'α helix) and C-terminal (Jα and Kα) to the LOV core domain. Blue-light absorption promotes reversible dissociation into two monomers. Notably, *Rs*LOV thus displays signal polarity opposite to that of several LOV photosensor domains, which undergo light-induced homo- or hetero-association (2,7,8). We reasoned that this unorthodox response to light could be exploited in photoreceptor engineering, via light-induced release of steric occlusion: in this approach, the *Rs*LOV photosensor

*To whom correspondence should be addressed. Tel: +49 30 2093 8845; Email: flosopher@gmail.com
Correspondence may also be addressed to Andreas Möglich. Tel: +49 921 55 7835; Email: andreas.moeglich@uni-bayreuth.de

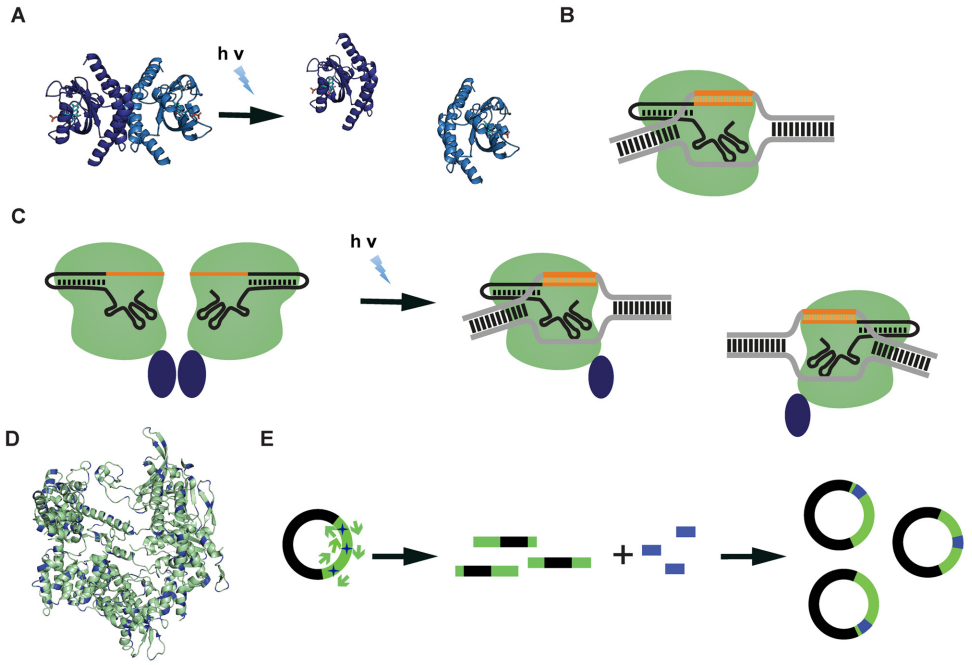

Figure 1. *Rs*LOV mechanism and creation of the (d)Cas9-*Rs*LOV domain insertion library. (**A**) The photoreceptor *Rs*LOV (PDB ID 4hj6) is a homodimer in the dark-adapted state but dissociates upon blue light exposure. (**B**) Cas9 is an RNA-guided DNA endonuclease. In the catalytically incapacitated form, dCas9 serves as an RNA-guided DNA binding protein. Cas9, gRNA, target DNA, and recognition sequence are shown in green, black, gray and orange, respectively. (**C**) Hypothetical mechanism of light regulation in a *Rs*LOV-(d)Cas9 chimera. In the dark-adapted dimeric state, the (d)Cas9 functional site is sterically blocked through dimerization via *Rs*LOV (dark purple ellipse). Light-induced dissociation leads to functional site release and restoration of activity. (**D**) 234 chosen insertion sites (blue) mapped onto the Cas9 apo structure (green, PDB ID 4cmp). (**E**) Cloning of a defined *Rs*LOV-dCas9 domain insertion library via Multiplex-Inverse PCR (MIP). For every insertion site, the dCas9 plasmid (green/black) is amplified with 'outward-facing' primers annealing at that site. The 'linearized' plasmids are then pooled and ligated with *Rs*LOV gene fragments (blue).

would be coupled with target effectors such that in the dark, unproductive dimeric complexes are formed with the effector active site sterically blocked. Light exposure would promote complex dissociation, release of steric occlusion and restoration of effector function.

To test these concepts, we selected the RNA-guided sequence-specific DNA endonuclease Cas9 from *Streptococcus pyogenes* (9) as the target effector because of its eminent biological relevance (10) and the availability of powerful screening assays. Cas9 can be programmed to cleave arbitrary DNA sequences with high specificity through a so-called guide-RNA (gRNA) reverse complementary to the target site (Figure 1B). This easy programmability has made Cas9 an indispensable tool for genome engineering across a wide range of organisms and tissues (11). Further, a catalytically inactive variant of Cas9, denoted dCas9, serves as a programmable, sequence-specific DNA-binding protein (12), thereby allowing precise control of transcriptional activity (12–14) and epigenetic modifications (15) of endogenous genetic loci. So far, only few natural mechanisms are known by which the molecular activity of CRISPR-Cas effectors are regulated (16), and the existence of naturally light-switchable (d)Cas9 variants appears unlikely. Such variants would be of interest for at least two reasons: (i) the 'classical' optogenetic premise of precise spatiotemporal control over cellular activities of interest (17); (ii) genome engineering efficiencies are hampered by off-target activity (18) and long DNA residence times (19). Cas9 variants with regulable activity might offer a way of mitigating these unwanted side effects.

In addition to split-Cas9 (20) and ligand-sensitive (21) Cas9 variants, two light-responsive Cas9 variants have recently been engineered. First, a critical lysine residue was modified with a photolabile protecting group, and Cas9 thereby inactivated (22). UV irradiation led to release of the protecting group and restoration of Cas9 activity. Although the light response showed a high dynamic range, the system is limited by the use of potentially harmful UV irradiation, irreversible photolysis of the protecting group and the need for incorporating unnatural amino acids. Second, Cas9 was split in two halves and linked to a heterodimeric LOV photoreceptor that reversibly associates upon light absorption (23). Activity of the split Cas9 protein could thus be regained in blue-light-regulated manner and with high dynamic range. This system relies on two separate polypeptide fragments, which might be of potential disadvantage in certain contexts (2).

A single-chain, light-regulated (d)Cas9 variant based on *Rs*LOV could hence be a valuable addition to the existing repertoire. To this end, we constructed a comprehensive domain-insertion library of variants where the *Rs*LOV photosensor is placed at different sites throughout the dCas9 gene. Screening by flow cytometry for light-induced differences in transcriptional repression yielded a (d)Cas9 variant moderately activated by blue light. As insertions of guest proteins frequently destabilize host proteins, we also screened the library for temperature dependence and iden-

tified another (d)Cas9 variant whose activity was strongly inhibited when elevating the temperature from 29 to 37°C. While lacking the excellent spatiotemporal control afforded by light, temperature variations offer an alternative means of perturbing cellular events reversibly and non-invasively, as we demonstrate by regulating expression from endogenous *Escherichia coli* promotors in temperature-dependent manner.

MATERIALS AND METHODS

dCas9 high-throughput assay

The *E. coli*-based assay system for dCas9 activity (Figure 2a, Supplementary Figure S1) consists of three separate plasmids. First, we subcloned the dCas9 gene into vector pCDF-Ara that harbors a streptomycin resistance marker and an arabinose–inducible promotor. Second, for use as a fluorescence reporter, we resorted to plasmid pROB12 (24), which confers kanamycin resistance and carries a dsRed-ExpressII expression cassette under control of the IPTG-inducible T7-lacO promotor. Third, to generate the sgRNA chassis, we assembled by PCR a linear construct containing a constitutive J23119 promotor (12), a specific 20nt gRNA sequence, and the 70nt constant sequence (9,12), and cloned this linear construct into a pACYC184 vector using HindIII/EagI sites. All enzymes were obtained from Fermentas (Thermo) or New England Biolabs. To enable multiplexing, a second J23119-sgRNA fragment was cloned into the same vector using BglI/EheI sites. To determine a sgRNA sequence yielding significant repression, we tried 5 different sequences in the 5′ region of the RFP gene (Supplementary Information, Figure S1, S2) in combination with dCas9. To run the assay, *E. coli* CmpX13 cells (25) carrying all three plasmids were grown to saturation without any induction. The culture was then diluted 1:100 (when assaying at 37°C) or 1:1000 (29°C), and dCas9 expression was induced with 3 mM arabinose. After 1 h (37°C) or 2 h (29°C), 1 mM IPTG was added to induce RFP expression. After an additional 4 h (37°C) or 15–16 h (29°C), RFP fluorescence was measured with a Tecan M200pro microplate reader (excitation 541 nm, emission 591 nm) and normalized by OD_{600}. Of the five sgRNAs tried (Supplementary Figure S2), the two that showed the highest repression levels (compared to empty sgRNA plasmid) were combined on one pACYC184 plasmid for multiplexing. As measured by flow cytometry, this double-sgRNA plasmid showed ∼350-fold repression of RFP expression (Figure 2b) compared to an empty pACYC184 plasmid, and was subsequently used during library screening.

Modeling and cloning of *Rs*LOV terminal extensions

To estimate the minimum number of residues necessary to bring the *Rs*LOV N- and C-termini into spatial proximity, we used the Rosetta3 (26) Remodel module (27) to model extensions of 16–22 amino acids on both the N- and C-termini of the *Rs*LOV crystal structure (5). Only the added residues were treated as flexible during the calculations. To guide sampling, a distance constraint of 6 Å was added between the N-terminal and C-terminal residues. Rosetta3 command lines and XML input files are in the SI note 3. For each extension length considered, 50 models were generated, and afterwards the number of models counted where the termini were within 6 Å of each other (Supplementary Figure S3 and Table S1). For N- and C-terminal extensions, a minimum number of 18 and 16 residues, respectively, was found to be necessary. Based on these results, and to ensure library diversity, we decided to generate variants with N- or C-terminal extensions of lengths 15, 20, 23, 26 and 29 residues, and also one variant carrying 15 residue extensions on both termini. To ensure the extensions were flexible, the sequence was chosen to consist of Gly/Ser/Ala/Thr repeats. All variants were generated by combining the *Rs*LOV gene, obtained as a gift from Brian Crane (5), with oligonucleotides encoding the extension sequence through PCR assembly.

Cloning the Cas9-*Rs*LOV 'Multiplex inverse PCR' (MIP) insertion library

The 234 insertion sites in Cas9 were chosen based on visual inspection of the apo crystal structure (28) (see SI note 4 for list). To build MIP-type insertion libraries (29), two problems need to be solved: (i) how to design the hundreds of primer sets and run the corresponding individual PCR reactions with manageable amount of labor; and (ii) how to efficiently ligate the linear vector and insert PCR fragments. For (i), we wrote a Python script (available at https://github.com/flosopher/floscripts/blob/master/genutils/InsertPrimerDesigner.py) that designs the two outward facing MIP primers for each site while attempting to keep the melting temperatures of both as similar as possible (Supplementary Figure S4). For (ii), we added NotI (at the 5′ *Rs*LOV fwd primer/Cas9 MIP rev primer) and SalI (*Rs*LOV 3′ rev primer / Cas9 MIP fwd primer) restriction sites to allow for efficient directional cloning. The restriction sites are translated as Ala-Ala-Ala (NotI) or Gly-Ser-Thr (SalI), ensuring that the linkers connecting the Cas9 insertion sites to the (extended) *Rs*LOV are flexible. The 234 primer pairs were ordered in 96-well plates, sorted row-wise by ascending melting temperature. PCR reactions for 231 primer pairs were successful. These were pooled, gel-purified (Macherey-Nagel PCR cleanup kit), and digested with NotI and SalI. In parallel, the 11 different *Rs*LOV linker/extension variants were amplified by PCR with primers containing NotI and SalI sites. The resulting products were pooled, treated with NotI/SalI, ligated to the digested dCas9 pool, transformed into NEB-5α (New England Biolabs) cells, and plated. To ensure good coverage of the $11 \times 231 = 2541$ theoretically expected variants in the library, enough transformation reactions for ∼20 000 colonies were carried out. Plasmids were prepared from these colonies (Macherey-Nagel plasmid isolation kit) and used to transform *E. coli* CmpX13 cells already containing the RFP reporter and gRNA plasmids.

Fluorescence-activated cell sorting (FACS) to identify switchable constructs

CmpX13 cells containing the dCas9-RsLOV insertion library plus RFP and gRNA plasmids were cultured as described above. Cultivation in the light was under 100 μW

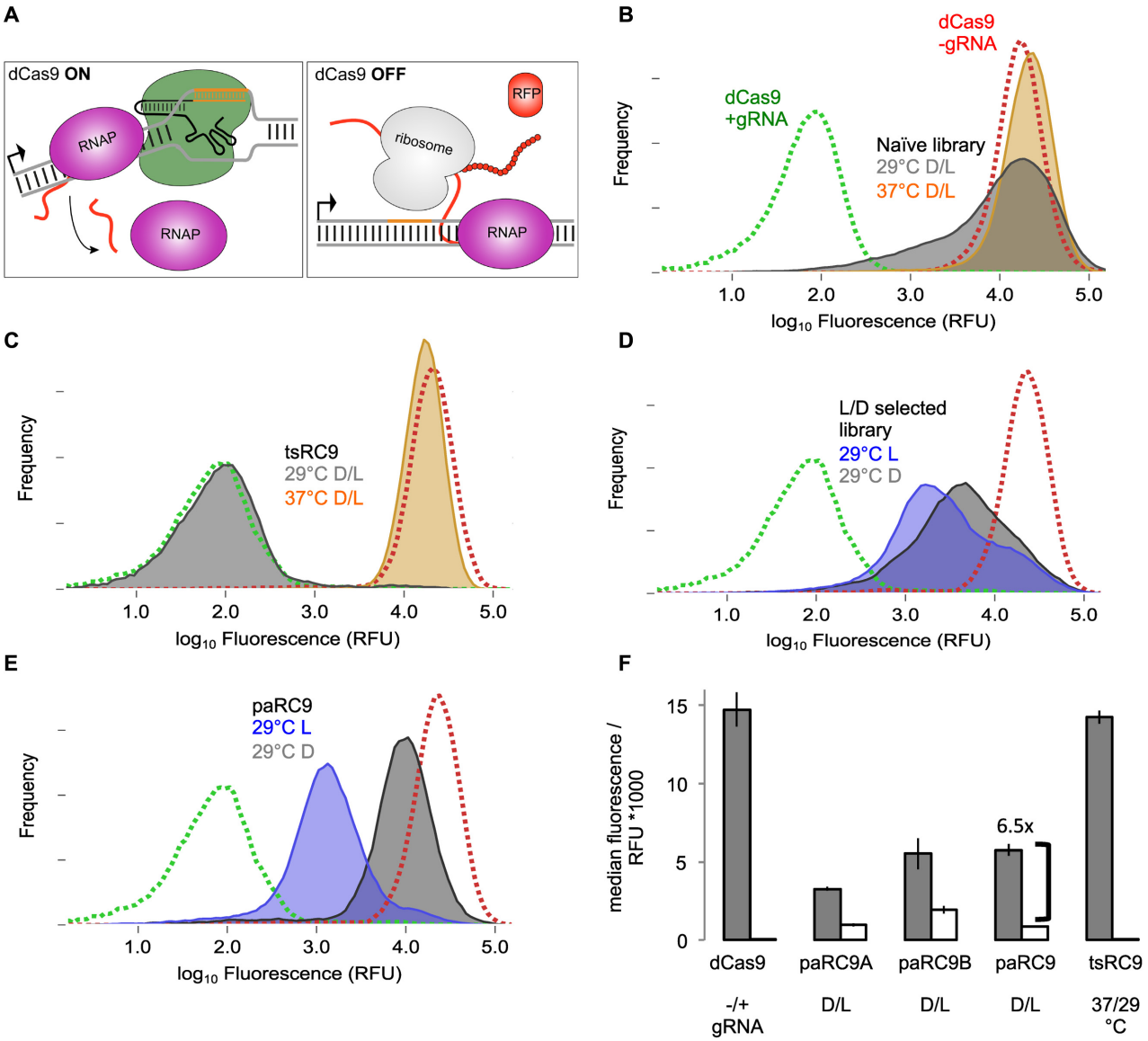

Figure 2. Screening of the *Rs*LOV-dCas9 insertion library for light- and temperature-switchable constructs. (**A**) Targeting of dCas9 to the 5′ coding region of an RFP reporter gene causes RNA polymerase (pink circle) to stall and results in reduced RFP expression. Switchable *Rs*LOV-dCas9 chimeras can thus be isolated by alternately screening for low and high fluorescence. (**B**) Fluorescence population of the naïve *Rs*LOV-dCas9 library at 37°C (orange) and 29°C (gray), with positive (dCas9 +gRNA, green) and negative (dCas9 –gRNA, red) controls shown for comparison. At 37°C, the library is virtually indistinguishable from the negative control population, indicative of most constructs being inactive. At 29°C, a broad shoulder towards the positive control population indicates the presence of several constructs functional at this lower temperature. (**C**) Isolation of tsRC9. After two rounds of screening for functional constructs at 29°C, tsRC9 was isolated, which shows dCas9-like activity at 29°C (gray) but virtually no activity at 37°C (orange). (**D**) Screening for light-switchable constructs. After 7 rounds of screening for high activity under blue-light irradiation (blue) and low activity in the dark (grey), constructs of intermediate activity were enriched and a small light/dark difference appeared. Two switchable constructs, paRC9A and B, were isolated from the enriched library. (**E**) Optimization of paRC9A. After computational modeling and screening of mutations stabilizing *Rs*LOV, a variant with improved repression under blue-light vs. dark conditions was obtained. (**F**) Median fluorescence values of all constructs from panels B-E. paRC9 has 6.5-fold dynamic range (shown are the mean and standard deviation (SD) of three individual measurements).

cm^{-2} 470 nm irradiation. After 16–19 h (29°C) or 4 h (37°C), cultures were chilled on ice, diluted 1:100 into ice-cold PBS buffer, and this suspension was analyzed and sorted on a BD FACS Aria II cell sorter. All events with a forward scatter area >4000 units and a sideward scatter area >7000 units were considered as cells. The PE-Texas-Red channel was used for RFP expression analysis. The negative control (dCas9, empty gRNA plasmid) had a peak at 1.6×10^4 RFU (relative fluorescence units), the positive control (dCas9 with gRNA) at $5*10^1$ RFU. (Figure 2B). The fluorescence range was thus divided into four regions: P1 (well working, fluorescence < 5×10^2 RFU), P2 (rather working, 5×10^2 RFU < fluorescence < 2×10^3 RFU), P3 (rather non-functional, 2×10^3 RFU < fluorescence < 8×10^3 RFU) and P4 (non-functional, fluorescence > 8×10^3 RFU). Three screening schemes were carried out:

P1L-P3D (meaning cells showing P1 fluorescence after being cultivated under blue light and P3 fluorescence after cultivation in darkness), P1L-P4D and P2L-P4D. A screening cycle consisted of selecting ∼30 000 cells cultured under blue light for low fluorescence (i.e. P1 or P2), sorting into fresh LB without inducers, growing to saturation, then diluting 1:1000 and induction/cultivation in darkness, followed by sorting 30 000 cells of high fluorescence (P3 or P4). paRC9A and B were isolated from the P2L-P4D population after seven sorting steps.

Cloning of the paRC9A linker library

The objective of this library was to simultaneously sample insertion site (Cas9 residues 468–481), linker length (7, 9, 12, 15, 19 amino acids), and linker sequence. We defined the minimum linker length (seven residues/21nt) on each side as an overlap for Gibson assembly (30), and ordered MIP-style primers carrying this overlap on their 5′ end for each of the 14 insertion points. Fourteen individual PCR reactions were carried out and the products pooled. For the *Rs*LOV inserts, five primers for each N- and C-terminus length were ordered consisting of the 5′ overlap sequence, a 3′ sequence complementary to the respective *Rs*LOV terminus, and an intermediate sequence of the respective length. For the primers to create linkers of 9, 12, 15, and 19 amino acids, one to two degenerate codons encoding four to eight different residues were added to the intermediate sequence. Twenty five PCRs (5 N-terminal primers * 5 C-terminal primers) for the *Rs*LOV inserts were done, which, when combined with the sequence degeneracy, yielded a total of 990 theoretical *Rs*LOV linker variants. The 25 products were pooled and combined with the MIP-PCR pool through Gibson assembly (30), yielding a library of theoretical size 14 000. Screening by FACS was carried out as described above.

Rosetta modeling of *Rs*LOV stabilizing mutations and cloning of the library

Modeling of mutations stabilizing the *Rs*LOV C-terminal helices was done analogously to the work of Guntas *et al.* (31). Briefly, at 50 positions in the intramolecular interface between the C-terminal helices and the central β-sheet, all residue identities observed at a given position in a BLAST alignment of *Rs*LOV were considered for mutation, leading to a total of 610 possible single point mutants. In addition, all double mutations within this set where the Cα atoms were within 10 Å of each other (a total of 42722) were also considered. The Rosetta3 pmut_scan protocol was used to calculate theoretical $\Delta\Delta G$ values for all 43332 single and double mutants, and models of mutants having a $\Delta\Delta G$ of <–0.3 Rosetta Energy units (REU) (single)/<–0.6 REU (double) were visually inspected (35 single and 102 double mutants). After visual inspection, a total of 16 mutations at 11 positions were chosen for incorporation into a library containing these point mutants and all combinations thereof, with a theoretical size of 13824 (Supplementary Table S2). Degenerate oligonucleotides containing the desired mutations were used to assemble the mutagenized *Rs*LOV gene (Supplementary Figure S5). Gibson overlaps at the N- and C-termini of *Rs*LOV were defined. A PCR with MIP-type primers carrying the same overlaps and with templates isolated from the linker library was run, and the resulting product combined with the mutated *Rs*LOV gene via Gibson assembly (30). Screening by FACS was carried out as described above.

β-Galactosidase assays

The sgRNAs against *lacZ* and *lacI* published by Qi *et al.* (12) were cloned into the pACYC184 plasmid and transformed into CmpX13 cells together with plasmids expressing paRC9, tsRC9 or dCas9. Cultures were grown to saturation without inducers, then diluted 1:100 into LB containing 1.5 mM arabinose to induce dCas9 variants and grown for 1 h. Then, 1 mM IPTG was added for samples containing *lacZ* gRNA, and the cultures were grown for another 4 h (37–35°C), 5 h (34–32°C) or 6 h (31–29°C). β-Galactosidase activity was quantified using the Pierce yeast β-galactosidase assay kit following the manufacturer's instructions.

Protein expression and purification

Escherichia coli CmpX13 were transformed with pCDF vectors expressing the C-terminally His-tagged paRC9 or tsRC9. 800 ml LB culture supplemented with 50 μM riboflavin and 35 μg/ml streptomycin were inoculated with 800 μl of overnight cultures and grown at 37°C and 225 rpm to an OD_{600} of 0.5. The cultures were chilled at 16°C and 225 rpm for 30 min prior to induction with 3 mM arabinose and incubation for 19 h at 16°C and 225 rpm. The cells were harvested at 4000 × g and 4°C for 10 min and resuspended in 20 ml lysis buffer (50 mM Tris–HCl pH 8.5, 300 mM NaCl, 10 mM imidazole and protease inhibitor cocktail Complete Ultra (Roche, Mannheim, Germany)). After lysis by sonication, the cleared lysate was purified by gravity-flow Co^{2+}-NTA affinity chromatography (HisPur Cobalt Resin, Thermo Scientific, Bonn, Germany). The protein was eluted with buffer containing 300 mM imidazole and dialyzed against 25 mM Tris HCl pH 8.5, 300 mM NaCl, 10% (v/v) glycerol. After concentration with a 50 kDa cutoff centrifugal filter device (Sartorius) protein concentration was quantified through the FMN cofactor peak at 450 nm using an extinction coefficient of 12 500 M^{-1} cm^{-1}, and aliquots were flash frozen and stored at −80°C.

Cleavage assays

Kinetic cleavage assays were performed by first preincubating Cas9 variants at 50 nM in KGB (32) under applicable light/temperature conditions (29°C or 37°C for tsRC9, dark or under blue light at 29°C for paRC9) for 10min, then adding 100 nM prehybridized dual-crRNA:tracrRNA of *Streptococcus pyogenes* targeting *speM* protospacer (33) and incubating for another 15min. Plasmid DNA containing *speM* was then added to a final concentration of 10 nM. After defined timepoints (1, 2, 5, 10, 20, 40 and 60 min) samples were withdrawn and the reaction was stopped by addition of 5× loading buffer (34). Cleavage reactions were analyzed by gelelectrophoresis on 0.8% agarose gels in 1× TAE and successive ethidium bromide staining. Percentage

of cleavage of at least three individual experiments was determined by densiometry and plotted against time.

Electrophoretic mobility shift assay

A 90-base pair PCR product containing *speM* protospacer was 5′ radiolabeled using [γ-^{32}P] ATP (Hartmann Analytics) and T4 polynucleotide kinase (Fermentas) according to the manufacturer's manual. The labelled substrate was purified using QIAquick PCR purification Kit (Qiagen). Cas9 variants were preincubated at applicable conditions (29°C or 37°C for tsRC9, dark or under blue light at 29°C for paRC9) in DNA-binding buffer (20 mM Tris HCl pH 7.4, 100 mM KCl, 5 mM $CaCl_2$, 1 mM DTT, 5% (w/v) glycerol, 20 ng/μl poly(dI-dC)) for 10 min, then mixed with two-fold molar excess of prehybridized dual-RNA and incubated for another 10 min followed by addition of 5 nM labelled DNA substrate. Binding reactions were then incubated for 1 h. The samples were loaded on a native 6% polyacrylamide gel, which was then run at 10 V cm^{-1} for 45 min in 0.5× TBE supplemented with 5 mM $CaCl_2$. The gels were exposed on autoradiography films and visualized by phosphorimaging. Percentage of bound DNA for at least three independent experiments was determined by densiometry and plotted against the protein concentration used (0, 15, 30, 40, 50, 60, 80, 100, 120, 200 nM). The apparent dissociation constant (K_D) was determined by least-squares fitting to the Hill equation (fraction bound = [protein]^n/($K_D{}^n$ + [protein]^n)).

RESULTS

Construction of a *Rs*LOV-Cas9 insertion library

We reasoned that the Cas9 effector could be rendered light-switchable if covalently linked with the *Rs*LOV photosensor such that in the dark, a dimeric complex with a sterically occluded functional site is formed (Figure 1C). Blue-light absorption would promote dissociation of the complex, and access to the functional site would be restored. To achieve this regulatory mechanism, photosensor and effector must be linked such that (i) their individual function and structures are only minimally perturbed; and ii) *Rs*LOV-mediated dimerization results in steric blockade of the Cas9 functional site. Despite the availability of high-resolution structures of both entities (5,28,35), chimeric constructs that meet these two criteria are hard to predict. We hence opted for construction of a library of *Rs*LOV inserted at several surface-exposed sites throughout the dCas9 effector, and for screening this library for light-regulated variants.

Inspection of the *Rs*LOV structure reveals its N- and C-termini to be separated by ∼40 Å (Supplementary Figure S3), meaning that insertion into Cas9 or other proteins would almost inevitably result in severe and detrimental structural distortions. To overcome this limitation, it is necessary to add linkers sufficiently long for bringing the termini into proximity. By computational design with flexible backbone geometry (27), we found that at least 18 N-terminal or 16 C-terminal residues are required to bridge the two termini (Supplementary Figure S3). We hence generated ten variants of *Rs*LOV with flexible linkers of 15, 20, 23, 26 or 29 residues appended at either N- or C-terminus, plus one variant featuring 15 residues at both termini. Next, based on visual inspection of the Cas9 crystal structure, we picked 234 surface-exposed positions as insertion points, on average corresponding to one insertion site for every 5.8 residues of Cas9 (Figure 1D). Combination of the 11 *Rs*LOV photosensor variants with the 234 Cas9 effector insertion sites, in theory gives rise to a library of 2574 unique *Rs*LOV-Cas9 chimeras. We cloned this library using the 'Multiplex Inverse PCR' (MIP) approach (Figure 1E) introduced by Ostermeier and co-workers (29). Successful library construction was confirmed by DNA sequencing of 25 random clones, which all represented different variants out of the 2574 theoretically expected.

High-throughput screening of *Rs*LOV-Cas9 activity

To facilitate library screening, we established an *E. coli*-based high-throughput assay following the CRISPR interference concept (CRISPRi) introduced by Qi *et al.* (12) and Bikard *et al.* (13). Here, the dCas9 variant, which is catalytically inactive, yet retains RNA-guided sequence-specific DNA binding, serves as a transcriptional repressor (Figure 2A). Directed to the promotor or 5′ region of a red-fluorescent reporter (RFP) gene, dCas9 interferes with transcription and thereby decreases expression of the target gene. If, however, dCas9 is left out or rendered unable to bind, transcriptional repression is relieved and high RFP reporter fluorescence is achieved. We adapted the setup by Qi *et al.* toward a three-plasmid system (Supplementary Figure S1), and found that in the presence of dCas9 and two gRNAs directed against the RFP, bacteria developed negligible fluorescence, indicative of efficient transcriptional repression. Omission of the gRNA yielded readily visible, approximately 350-fold elevated fluorescence (Figure 2B and F, SI, Figure S2). Of particular advantage, the RFP repression assay lends itself to fluorescence-activated cell sorting (FACS) of the *Rs*LOV-dCas9 libraries and allows isolation of clones harboring either binding-proficient dCas9 variants (screening for low fluorescence) or binding-deficient dCas9 variants (screening for high fluorescence). In iterative rounds, the *Rs*LOV-dCas9 libraries were cultured under alternating blue-light and dark conditions, and *E. coli* cells were alternately sorted for low and high RFP fluorescence, respectively.

Identification of temperature-sensitive and light-regulated *Rs*LOV-(d)Cas9 variants

Following cultivation at 29°C in darkness or constant blue light (470 nm, 100 μW cm^{-2}), the naïve *Rs*LOV-dCas9 library was analyzed by FACS (Figure 2B). As expected for domain insertions (29), a large fraction of the variants in the initial naïve library were not functional, indicated by a dominant peak at high fluorescence that corresponds to a negative control (dCas9 without gRNA). A broad tail toward lower fluorescence values, corresponding to a positive control (dCas9 with gRNA), suggested that several variants were at least partially functional. No light/dark difference was visible in the initial library. When grown at 37°C, the naïve library displayed fluorescence levels almost identical to the negative control, indicating that the vast

majority of variants in the library are binding-deficient at 37°C, in contrast to the findings at 29°C. Evidently, the library comprised constructs with strongly temperature-dependent dCas9 activity. Following two rounds of screening for efficient repression at 29°C, we isolated a variant, denoted tsRC9 (temperature-sensitive *Rs*LOV-Cas9), in which *Rs*LOV with a C-terminal linker of 21 residues is inserted between residues N235 and G236 (Supplementary Figure S6). tsRC9 is as competent as dCas9 at inhibiting RFP expression at 29°C, but shows no repression activity at 37°C (Figure 2C and F). Blue light had no effect on transcriptional repression by tsRC9. To investigate whether the observed temperature-sensitivity is due to an intrinsic property of *Rs*LOV or is caused by perturbation of the (d)Cas9 structure around position 235, we created and tested variant tsRC9_GFPex. In this variant, the *Rs*LOV insert is exchanged for superfolder GFP (sfGFP), a single-domain protein of comparable size to RsLOV and generally considered stable. tsRC9_GFPex shows negligible temperature-sensitivity (Supplementary Figure S10), indicating that the properties of tsRC9 are due to the *Rs*LOV insert. This view is further corroborated by the observation of a substantial fraction of temperature-sensitive variants in the naïve *Rs*LOV-dCas9 library.

To isolate a light-activatable *Rs*LOV-Cas9 construct, we alternately screened the naïve library for cells displaying low fluorescence after incubation under blue light (at 29°C), followed by screening for cells displaying high fluorescence after incubation in the dark. After seven rounds of screening (4× light, 3× dark), the library showed a small but reproducible difference between dark and blue-light conditions (Figure 2D), indicating enrichment of light-activated constructs. Testing of individual clones from the enriched library yielded two clones, denoted paRC9A (photoactivatable *Rs*LOV-Cas9 A) and paRC9B, that both showed repression activity that was enhanced under blue light by factors of 3.4 (paRC9A) and 2.8 (paRC9B). DNA sequencing revealed that in paRC9A, *Rs*LOV (with linkers of 15 residues at both termini) had been inserted between residues F478 and E479 (Supplementary Figure S6), into a loop that is disordered in the apo structure of Cas9 but mediates important interactions with the gRNA (28,35). In paRC9B, *Rs*LOV (with a 24-residue N-terminal linker) had been inserted between residues S1088 and M1089, in a domain of Cas9 that contacts the 3′ end of the gRNA (Supplementary Figure S6) (28,35). Notably, in all three isolated constructs, *Rs*LOV was inserted at Cas9 positions that were found to be tolerant to domain insertion in a recent Cas9 engineering study (21).

Improving the dynamic range of paRC9A

The activity difference (dynamic range) between 29 and 37°C observed for tsRC9 is on par with the activity difference between the dCas9 +gRNA positive and the dCas9 −gRNA negative controls. Hence, tsRC9 likely cannot be much improved nor does it need to be. By contrast, the dynamic range of paRC9A/B needs to be enhanced before becoming useful in applications. In the past, engineered photoreceptors were improved in their dynamic range by optimization of the photosensor itself (31) or by modulation of the linkers connecting photosensor and effector (36,37). We focused on optimizing paRC9A because of its higher dynamic range compared to paRC9B and because of initial experiments indicating it was more optimizable (Supplementary Figure S7).

We first varied the position at which *Rs*LOV is inserted into dCas9 as well as linker length and composition. To this end, we constructed a library where the *Rs*LOV photosensor was inserted at any of the 14 surface-exposed positions between K468 and V481 of dCas9. Moreover, a set of N- and C-terminal linkers with 7, 9, 12, 15 or 19 residues were used, and additional linker sequence diversity was introduced via PCR amplification with degenerate oligonucleotide primers. Altogether, the theoretical library size amounted to 14 000. Even after 10 rounds of screening (cf. above), we failed to identify any significantly improved variants; however, although none of the library members had improved dynamic range, some showed lower or higher RFP repression levels than paRC9A (Supplementary Table S3, Figure S8).

We next reasoned that the dark activity of paRC9A could be lowered and thus the dynamic range enhanced by stabilizing the *Rs*LOV photosensor dimer interface formed by the A'α, Jα and Kα helices. Analogous to a recent engineering study on the *Avena sativa* phototropin1 LOV2 photosensor (31), we used computational modeling to identify stabilizing mutations at the interface between these helices and the central β–sheet of *Rs*LOV. We thus selected 16 potentially stabilizing mutations at 11 residue positions and incorporated them in a combinatorial library containing 13824 different *Rs*LOV variants (Supplementary Table S2). This library was combined with 10 variants isolated from the previous, linker-based optimization round, thus yielding a total library of ∼138 000 variants. Twelve rounds of screening identified a construct (paRC9 from hereon) with around two-fold improved dynamic range of 6.5 (Figure 2E and F). The improvement was due to decreased dark-state activity, in line with the design hypothesis. Sequencing of paRC9 revealed it to have four residue exchanges (Q82V, H102F, A164S, L168M in *Rs*LOV numbering) relative to wild-type *Rs*LOV, thereby resulting in a more hydrophobic sheet/helix interface (Supplementary Figure S9).

As controls, we created variants C548A (equivalent to C55A in *Rs*LOV) and Q611A (Q118A) of paRC9, thus replacing two residues in the *Rs*LOV photosensor that are critical for photochemistry and signal transduction (5,6,38). The response to light was greatly diminished in these variants (Supplementary Figure S10), ascertaining that light-sensitivity in paRC9 necessitates intact photochemical reaction of the *Rs*LOV photosensor.

Switchable DNA cleavage by tsRC9 and paRC9 in *E. coli*

Although efficient with a throughput of $\sim 10^7$–10^8 (limited by cloning efficiency and event rate of the flow cytometer), the above dCas9 screening assay has the drawback of being based on DNA binding rather than cleavage. To ascertain whether tsRC9 and paRC9 possess switchable DNA cleavage activity, we also tested these variants in the catalytically active Cas9 background. Within the above *E. coli*-based assay system, Cas9-mediated DNA cleavage would lead

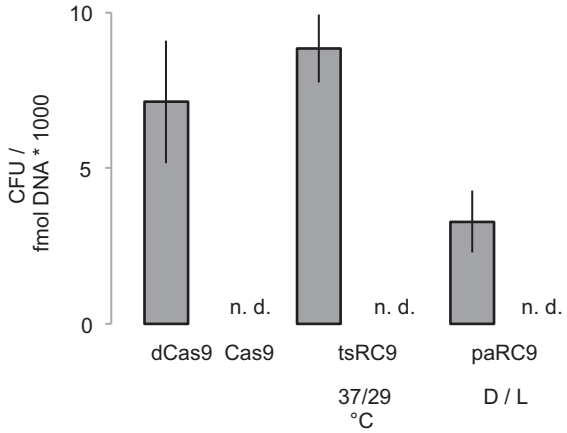

Figure 3. Cleavage activity of paRC9 and tsRC9 in *E. coli*. paRC9 and tsRC9 were co-expressed in the cleavage-competent Cas9 context with a gRNA targeting a plasmid conferring kanamycin-resistance. Plating on selective media under the respective 'off' condition (37°C for tsRC9, dark for paRC9) yielded colonies at counts similar (tsRC9) or reduced (paRC9) compared to dCas9, but no colonies (n.d. = not detected) in the respective 'on' condition (29°C for tsRC9, 30 μW cm^{-2} 470 nm light for paRC9). Shown are mean ± SD of three individual experiments.

to degradation of the RFP-expressing plasmid which confers resistance to kanamycin. When grown on kanamycin-containing agar plates, clones expressing a Cas9 control accordingly did not grow but those expressing the cleavage-incompetent dCas9 control formed colonies (Figure 3). When testing paRC9 in this assay, bacterial colonies only formed under dark conditions, although at reduced size and count (CFU, colony-forming units) compared to the dCas9 control. These results indicate light-activated cleavage activity of paRC9. In case of tsRC9, CFU counts comparable to dCas9 were observed at 37°C (although colonies were smaller), but no colonies were visible after incubation at 29°C. These results suggest that tsRC9 shows strongly temperature-switchable cleavage activity, but in contrast to the RFP repression case, there seems to be residual activity at 37°C.

Biochemical investigation of DNA binding and cleavage by tsRC9 and paRC9

Having isolated tsRC9 and paRC9, we next investigated whether the activities of these variants are allosterically regulated at the molecular level, or whether they constitute so-called 'phenotypic' switches that show switchable activity in cellular but not in biochemical assays. Previous efforts to develop switchable proteins by combining sensor and effector domains (39,40) have yielded both 'true' allosteric molecules as well as 'phenotypic' constructs. Activity differences of the latter can often be attributed to increased cellular protein accumulation in the 'on' condition of the switch (40).

We expressed and purified paRC9 and tsRC9 in the cleavage-competent Cas9 background. Absorption spectroscopy confirmed correct incorporation of the flavin chromophore and intact LOV photochemical response. We first performed cleavage assays with dual crRNA:tracrRNA directed against a unique target site within a 7700 base-pair supercoiled plasmid. At 29°C, tsRC9 readily catalyzed DNA cleavage, albeit at about 4-fold reduced activity compared to wild-type Cas9. At 37°C, catalytic activity of tsRC9 was around 12-fold lower than at 29°C (Figure 4A and B). Experiments with paRC9 showed DNA cleavage at 7-fold reduced rate compared to wild-type Cas9, independent of whether experiments were conducted under dark or blue-light conditions (Figure 4B, representative gels in Supplementary Figure S11). We next assessed affinity for a DNA target site in electrophoretic mobility shift assays (EMSA). tsRC9 and paRC9 were incubated in presence of dual crRNA:tracrRNA directed against a 90 base-pair linear double-stranded DNA fragment. At 29°C, tsRC9 showed tighter DNA binding than at 37°C, with apparent affinities of 44.3 ± 2.9 nM and 95.4 ± 7.7 nM, respectively (Figure 4C and D). For paRC9, in line with the DNA cleavage experiments, no light/dark difference was observed, with apparent affinities of 73.9 ± 10.2 nM under light and 74.4 ± 13.4 nM under dark conditions (Figure 4D, representative gels in Supplementary Figure S11). For wild-type Cas9, an apparent affinity of 40.5 ± 5.9 nM was observed for the substrate used (Supplementary Figure S11b). Notably, all three proteins showed high degrees of cooperativity.

These results suggest that paRC9 is a phenotypic switch, while tsRC9 is inherently temperature-sensitive. However, for tsRC9 there is also a discrepancy between the dynamic ranges observed in *E. coli* (∼300-fold) and in biochemical assays (2- and 12-fold). This could indicate that a combination of molecular properties and protein accumulation is responsible for the full intracelluar effect, but there are also other possible explanations for these discrepancies. First, the short linear relaxed substrate used in the EMSA experiments is rather unnatural in that Cas9 apparently displays higher reactivity towards negatively-supercoiled DNA (9). Second, in a typical cellular setting, Cas9 needs to find its target against a background of thousands of other plasmid and genomic protospacer-adjacent-motif (PAM) sites that are also sampled (41), while fewer 'decoy'-PAMs were present in the cleavage and EMSA experiments. Third, the repressional effect on gene expression might be subject to cellular amplification mechanisms and may hence scale non-linearly with DNA-binding and DNA-cleavage activities.

To investigate the nature of the observed temperature dependency of tsRC9, we performed thermal unfolding experiments monitored by circular-dichroism (CD) spectroscopy (Supplementary Figure S12, Table S4). A possible explanation for the properties of tsRC9 would be global unfolding between 29°C and 37°C. However, the observed melting point of tsRC9 was 42.7°C, while wild-type Cas9 melted at 44.2°C. Although insertion of *Rs*LOV apparently has a small effect on global stability, these data rule out global unfolding as a cause for the temperature sensitivity of tsRC9. Because the isolated RsLOV domain had a melting point of 53.4°C, complete unfolding of the *Rs*LOV insert in tsRC9 between 29 and 37°C is not likely either. Finally, to assess whether differences in protein expression play a role in paRC9 or tsRC9, we probed expression levels under assay conditions by Western blot (Supplementary Figure S13). The data indicate that both paRC9 and tsRC9 show similar

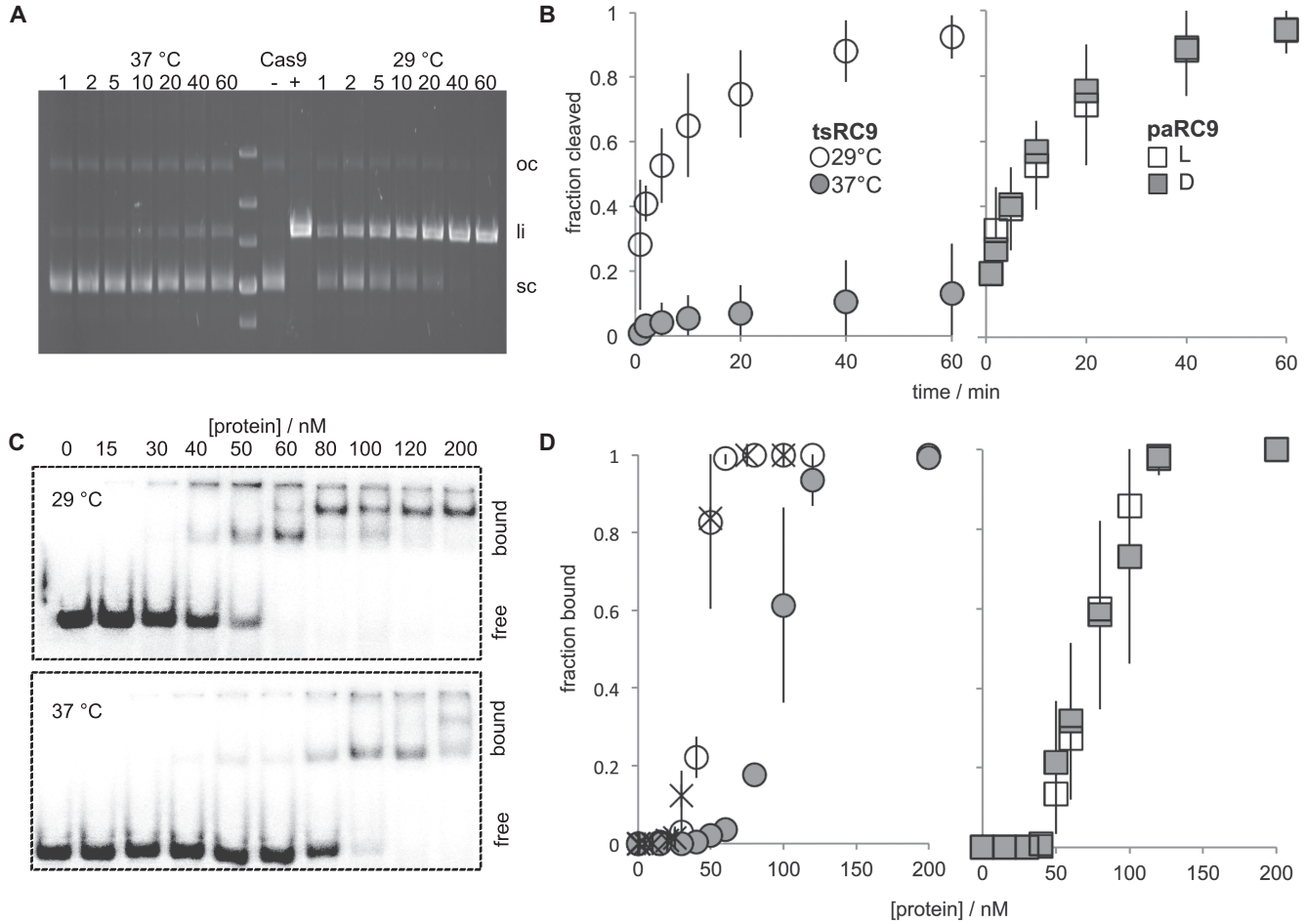

Figure 4. Biochemical investigation of tsRC9 and paRC9 DNA cleavage and binding activity. (**A**) tsRC9 cleavage of a plasmid-encoded target site at 29 and 37°C. In the initial plasmid preparation, bands for the supercoiled (sc) and open-circular (oc) species are detected. Incubation with 50nM Cas9 for 1 h at 37°C leads to complete digestion and a single band for the linear double-stranded species (li). Incubation with tsRC9 for 1, 2, 5, 10, 20, 40 and 60 minutes shows faster cleavage at 29°C than at 37°C. (**B**) Quantification of cleavage experiments for tsRC9 and paRC9 ($n = 3$, mean ± SD). For tsRC9, a ∼12× difference in initial reaction velocity is observed between 29°C (open circles) and 37°C (gray circles), while paRC9 shows no light-induced difference in cleavage activity (open and gray squares). (**C**) Electrophoretic mobility shift assay (EMSA) for tsRC9 and a 90nt linear dsDNA (5nM concentration) at 29°C and 37°C. Free and bound DNA are indicated. (**D**) Quantification of EMSA experiments for tsRC9 and paRC9 ($n = 3$, mean ± SD) A ∼2-fold increased affinity is observed at 29°C versus 37°C for tsRC9, while paRC9 has identical affinities in light and dark. Crosses are data for wild-type Cas9.

overall expression in their respective on- (light for paRC9, 29°C for tsRC9) and off-conditions (dark for paRC9, 37°C for tsRC9).

Regulation of endogenous genes with paRC9 and tsRC9

As paRC9 and tsRC9 were isolated based on repression of plasmid-encoded genes, we next assessed to what extent different endogenous genes can be regulated in their expression with these constructs. To this end, we tried gRNAs that target two genes of the well-characterized *E. coli lac* operon: *lacZ* encoding the enzyme β-galactosidase, and *lacI* encoding the regulatory LacI repressor which blocks transcription of *lacZ* by binding to an upstream operator site O (12). Presence of lactose or the non-hydrolyzable analog IPTG induces LacZ expression by binding to LacI and causing it to dissociate from the O site. Qi *et al.* previously showed that a gRNA designed to repress LacZ expression completely abolished β-galactosidase activity even in the presence of IPTG; by contrast, a gRNA against *lacI* induced β-galactosidase activity even in the absence of IPTG, albeit not by as much as regular IPTG induction.

As a positive control, we used dCas9 and reproduced the findings by Qi *et al.* (12) for gRNAs directed against the *lacI* and *lacZ* genes (Figure 5A). For paRC9 with the *lacZ* gRNA in the presence of IPTG, we observed no repression of β-galactosidase activity in the dark but a 3-fold repression in the light. When testing paRC9 with *lacI* gRNA in the absence of IPTG, β-galactosidase activity was induced neither in the dark nor light (Figure 5A), indicating that paRC9 fails to sufficiently repress *lacI*. We note that the LacI repressor is a regulatory transcription factor, meaning a few molecules per cell suffice to permanently occupy the single-copy O site and repress β-galactosidase expression. β-Galactosidase activity is hence not expected to scale linearly with LacI expression but rather show cooperative or even step-wise dependency.

For tsRC9 with *lacZ* gRNA in the presence of IPTG, complete β-galactosidase repression was observed at 29°C,

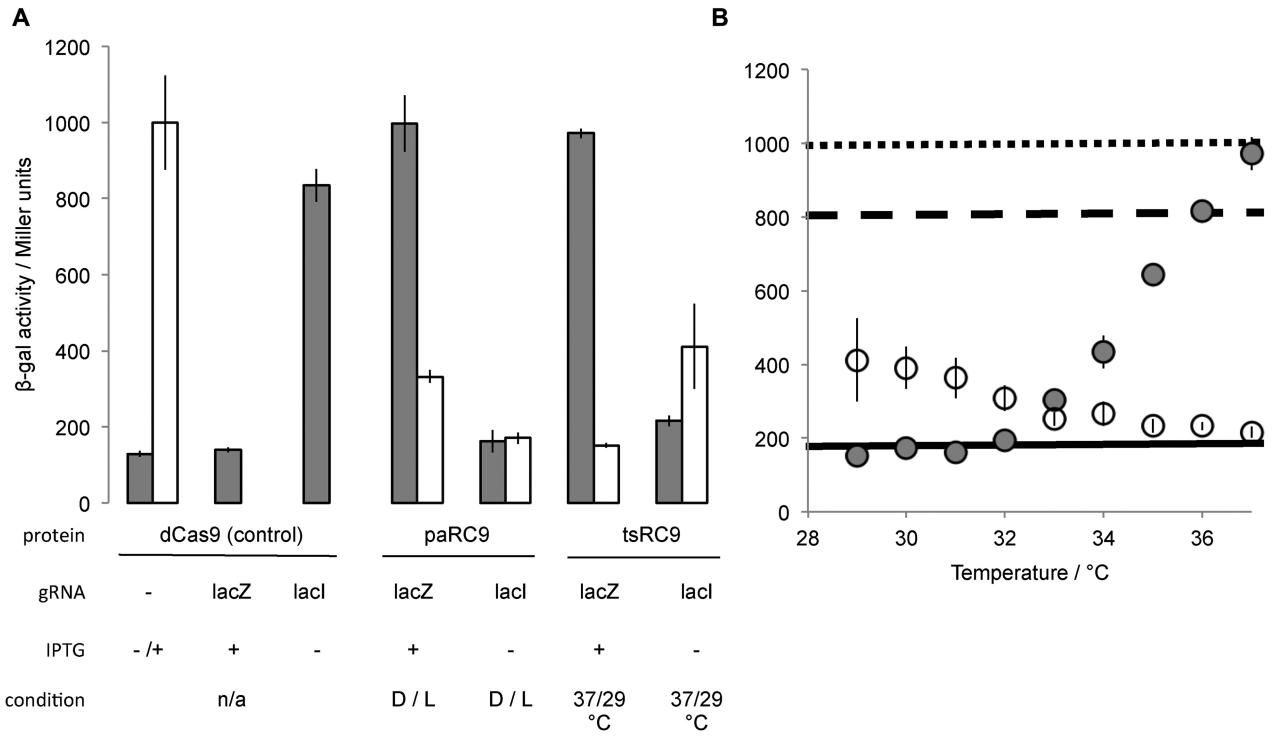

Figure 5. Repression of endogenous genes by tsRC9 and paRC9. (**A**) Transcriptional repression of genes from the *lac* operon was assessed by measuring β-galactosidase (βgal) activity. Using a gRNA directed against the *lacZ* structural gene, tsRC9 completely represses βgal activity at 29°C, despite the presence of the inductor IPTG. No repression is observed at 37°C. With paRC9, no repression is observed in dark, but about 3-fold repression under blue light. Using a gRNA directed against the gene encoding the LacI repressor, in the absence of IPTG, tsRC9 partly represses the LacI repressor at 29°C, but not at 37°C. paRC9 shows no effect in either light or dark with this gRNA. Shown are mean ± SD of three individual experiments. (**B**) Temperature series of tsRC9-induced repression showing that repression activity can be fine-tuned by growth temperature. βgal-activity with *lacZ* gRNA (+IPTG) is shown in gray circles, activity with *lacI* gRNA in open circles. βgal-activity levels at full IPTG induction (dotted line), no induction (thick line), and at dCas9 +*lacI* gRNA-mediated induction (dashed line) are shown for comparison. Shown are mean ± SD of three individual experiments.

but no repression was seen at 37°C. Using tsRC9 together with *lacI* gRNA in the absence of IPTG, at 29°C β-galactosidase activity was induced by about half as much as for dCas9 but not at all at 37°C (Figure 5A). These results are consistent with the above finding for the plasmid-based RFP gene that tsRC9 has similar repression activity as dCas9 at 29°C but no detectable activity at 37°C. To better characterize the temperature dependency of tsRC9, we also measured repression activities with *lacZ* and *lacI* gRNAs at a range of temperatures between 29 and 37°C (Figure 5B). In case of the *lacZ* gRNA, repression of β-galactosidase activity by tsRC9 was comparable to dCas9 for 32°C and lower temperatures but gradually attenuated at higher temperatures and was completely lost at 37°C. For the *lacI* gRNA, β-galactosidase induction gradually decreased between 29 and 33°C, with no induction at higher temperatures. These data suggest that tsRC9 can be used to fine-tune expression levels of endogenous genes by culturing bacteria at suitable temperatures.

DISCUSSION

In this work, we explored whether the *Rs*LOV photosensor can render an unrelated effector light-switchable, with Cas9 as the proof-of-principle target. Using a comprehensive domain-insertion library in combination with high-throughput screening, we isolated the paRC9 variant that showed light-switchable (d)Cas9 activity in three different *E. coli*-based assays, namely plasmid cleavage, repression of plasmid-encoded genes and repression of endogenous genetic loci. Removal of key residues engaged in LOV photochemistry largely abolished light regulation, indicating that light-sensitivity of paRC9 is indeed dependent on the integrity of the *Rs*LOV insert. However, biochemical DNA cleavage and binding experiments failed to identify light-regulated activity in paRC9 under the conditions investigated. Rather, paRC9 appears to be a phenotypic switch that only manifests its switching properties in the cellular context. Strikingly, from the same *Rs*LOV-Cas9 library we also isolated a construct with strong temperature-dependent activity, both when tested in *E. coli* and in biochemical assays. While destabilization of proteins through insertion of other domains is well known, the complete loss of initial wild-type-like activity within a rather small window of 4–5°C (Figure 5B) in tsRC9 is remarkable. To our knowledge, tsRC9 represents the first case where a photosensor bestows temperature sensitivity, and also the first report of a temperature-sensitive Cas9 variant. These results bring up two principal questions: (i) can *Rs*LOV be used to make other effector proteins light- and temperature sensitive; and (ii) are paRC9 and/or tsRC9 useful for applications?

We are cautiously optimistic that *Rs*LOV can confer temperature-sensitivity onto other effectors. In the naïve library, essentially every construct was devoid of activity at 37°C, indicating that the temperature sensitivity is independent of insertion site and likely not predicated on specific interactions between *Rs*LOV and Cas9. Moreover, replacing *Rs*LOV with sfGFP largely abolished temperature-sensitivity of tsRC9. These observations, combined with the fact that a temperature effect is observed in biochemical assays, suggest that the temperature sensitivity is rooted in *Rs*LOV itself. The transition window between ∼30°C and 37°C would allow for a wide range of applications. More studies are necessary, but *Rs*LOV could serve as a temperature-based 'destabilizing domain', analogous to the ligand-based FKBP system (42).

Regarding the light dependence of paRC9, the situation is less clear-cut. As a phenotypic switch, the light-dependent activities observed in *E. coli* require the presence of other cellular components, and may not be related to *Rs*LOV dimerization. In the naïve library, light dependence was apparently restricted to two insertion sites, and shifting the paRC9A insertion site by three residues led to high constitutive activity (Supplementary Figure S7), which suggests that the observed behavior requires a particular orientation of *Rs*LOV relative to Cas9. Initial experiments (Supplementary Figure S13) indicate that differences in protein accumulation (which has been implicated for other phenotypic switches) (39) are not responsible for the observed activity difference. One hypothesis that could explain these data is that the different molecular shape of *Rs*LOV (5) in the light state causes paRC9 to interact differently with cellular constituents, as has been shown for other proteins (43). However, as the identity of the other required factors is unclear, there are no simple experiments to prove or disprove this hypothesis. Thus, while paRC9 shows that *Rs*LOV can confer light-sensitivity to an arbitrary effector, the mechanism and transferability to other effectors remain unclear.

In terms of practical applicability, we believe that tsRC9 could be useful in several (d)Cas9 application scenarios, while paRC9 is probably mostly suited for bacterial transcriptional repression. In case a desired biological effect can be obtained by a 3–6-fold difference in protein expression, the single-chain paRC9 would be the tool of choice vis-à-vis the other published light-switchable Cas9 constructs. For tsRC9, we have demonstrated efficient repression of plasmid- and chromosome-based loci in *E. coli*, with the possibility of fine-tuning expression level by growth temperature. While repression for *lacI*, and by implication other regulatory loci, is not complete, this could be improved by multiplexing with several gRNAs (12). To our knowledge, tsRC9 represents the first system to enable temperature-sensitive, likely reversible and programmable knockdown of arbitrary target genes in *E. coli* and possibly other prokaryotes, with multiple potential applications in synthetic biology and bacterial genetics (44,45). As tsRC9 shows temperature-sensitive DNA binding, other dCas9 mediated transcription-level applications (such as upregulating genes through dCas9-activation domain fusions) can likely also be achieved (13), although the dynamic ranges observed in the present study may not be directly transferable. tsRC9 could also be applied to transcriptional regulation in eukaryotic cells (14), provided that the system under study can withstand prolonged periods at ∼30°C. When considering cleavage applications, we note that tsRC9 still shows residual activity at 37°C in the biochemical and *E. coli* cleavage assays. Thus, a scenario that relies on robust activity at 29°C, but complete prevention of even single cleavage events at 37°C is likely not achievable with tsRC9. However, tsRC9 might offer new avenues towards preventing problems related to off-target cleavage and post-cleavage DNA release (18,19).

SUPPLEMENTARY DATA

Supplementary Data are available at NAR Online.

ACKNOWLEDGEMENTS

We are grateful to Brian Crane and Karen Conrad (Cornell U) for the *Rs*LOV gene, Christiane Müller(Humboldt University) for flow-cytometry support, Carlos Gasser (Humboldt University) for help with Western blotting, and Peter Hegemann (Humboldt University) for providing laboratory space and equipment. We appreciate helpful discussions with Oliver Daumke (MDC Berlin) and members of the Möglich and Charpentier groups.

FUNDING

Deutsche Forschungsgemeinschaft (RI2468/1-1 to F.R.); Sofja-Kovalevskaya Award (to A.M.) and AvH Professorship (to E.C.) by the Alexander-von-Humboldt Foundation; Einstein Foundation Berlin (IPF-2012-148 to F.R. & A.M.); German Federal Ministry for Education and Research; Helmholtz Association; Max Planck Society; the Göran Gustafsson Foundation (Göran Gustafsson Prize from the Royal Swedish Academy of Sciences); Swedish Research Council and Umeå University (all to E.C.). Funding for open access charge: Humboldt-University Berlin and University of Bayreuth.

Conflict of interest statement. E.C. is a co-founder of CRISPR Therapeutics AG and ERS Genomics, and is a member of the scientific advisory board of CRISPR Therapeutics AG and Horizon Discovery Group.

REFERENCES

1. Möglich,A., Yang,X., Ayers,R.A. and Moffat,K. (2010) Structure and function of plant photoreceptors. *Annu. Rev. Plant Biol.*, **61**, 21–47.
2. Ziegler,T. and Möglich,A. (2015) Photoreceptor engineering. *Front. Mol. Biosci.*, **2**, 30.
3. Harper,S.M., Neil,L.C. and Gardner,K.H. (2003) Structural basis of a phototropin light switch. *Science*, **301**, 1541–1544.
4. Kennedy,M.J., Hughes,R.M., Peteya,L.A., Schwartz,J.W., Ehlers,M.D. and Tucker,C.L. (2010) Rapid blue-light-mediated induction of protein interactions in living cells. *Nat. Methods*, **7**, 973–975.
5. Conrad,K.S., Bilwes,A.M. and Crane,B.R. (2013) Light-Induced Subunit Dissociation by a Light–Oxygen–Voltage Domain Photoreceptor from Rhodobacter sphaeroides. *Biochemistry*, **52**, 378–391.
6. Conrad,K.S., Manahan,C.C. and Crane,B.R. (2014) Photochemistry of flavoprotein light sensors. *Nat. Chem. Biol.*, **10**, 801–809.

7. Yazawa,M., Sadaghiani,A.M., Hsueh,B. and Dolmetsch,R.E. (2009) Induction of protein-protein interactions in live cells using light. *Nat. Biotechnol.*, **27**, 941–945.
8. Wang,X., Chen,X. and Yang,Y. (2012) Spatiotemporal control of gene expression by a light-switchable transgene system. *Nat. Methods*, **9**, 266–269.
9. Jinek,M., Chylinski,K., Fonfara,I., Hauer,M., Doudna,J.A. and Charpentier,E. (2012) A programmable dual-RNA–guided DNA endonuclease in adaptive bacterial immunity. *Science*, **337**, 816–821.
10. Doudna,J.A. and Charpentier,E. (2014) Genome editing. The new frontier of genome engineering with CRISPR-Cas9. *Science*, **346**, 1258096.
11. Wright,A.V., Nuñez,J.K. and Doudna,J.A. (2016) Biology and applications of CRISPR systems: harnessing nature's toolbox for genome engineering. *Cell*, **164**, 29–44.
12. Qi,L.S., Larson,M.H., Gilbert,L.A., Doudna,J.A., Weissman,J.S., Arkin,A.P. and Lim,W.A. (2013) Repurposing CRISPR as an RNA-guided platform for sequence-specific control of gene expression. *Cell*, **152**, 1173–1183.
13. Bikard,D., Jiang,W., Samai,P., Hochschild,A., Zhang,F. and Marraffini,L.A. (2013) Programmable repression and activation of bacterial gene expression using an engineered CRISPR-Cas system. *Nucleic Acids Res.*, **41**, 7429–7437.
14. Konermann,S., Brigham,M.D., Trevino,A.E., Joung,J., Abudayyeh,O.O., Barcena,C., Hsu,P.D., Habib,N., Gootenberg,J.S., Nishimasu,H. *et al.* (2015) Genome-scale transcriptional activation by an engineered CRISPR-Cas9 complex. *Nature*, **517**, 583–588.
15. Thakore,P.I., D'Ippolito,A.M., Song,L., Safi,A., Shivakumar,N.K., Kabadi,A.M., Reddy,T.E., Crawford,G.E. and Gersbach,C.A. (2015) Highly specific epigenome editing by CRISPR-Cas9 repressors for silencing of distal regulatory elements. *Nat. Methods*, **12**, 1143–1149.
16. Bondy-Denomy,J., Garcia,B., Strum,S., Du,M., Rollins,M.F., Hidalgo-Reyes,Y., Wiedenheft,B., Maxwell,K.L. and Davidson,A.R. (2015) Multiple mechanisms for CRISPR-Cas inhibition by anti-CRISPR proteins. *Nature*, **526**, 136–139.
17. Deisseroth,K. (2015) Optogenetics: 10 years of microbial opsins in neuroscience. *Nat. Neurosci.*, **18**, 1213–1225.
18. Nuñez,J.K., Harrington,L.B. and Doudna,J.A. (2016) Chemical and biophysical modulation of Cas9 for tunable genome engineering. *ACS Chem. Biol.*, **11**, 681–688.
19. Richardson,C.D., Ray,G.J., DeWitt,M.A., Curie,G.L. and Corn,J.E. (2016) Enhancing homology-directed genome editing by catalytically active and inactive CRISPR-Cas9 using asymmetric donor DNA. *Nat. Biotechnol.*, **34**, 339–344.
20. Zetsche,B., Volz,S.E. and Zhang,F. (2015) A split-Cas9 architecture for inducible genome editing and transcription modulation. *Nat. Biotechnol.*, **33**, 139–142.
21. Oakes,B.L., Nadler,D.C., Flamholz,A., Fellmann,C., Staahl,B.T., Doudna,J.A. and Savage,D.F. (2016) Profiling of engineering hotspots identifies an allosteric CRISPR-Cas9 switch. *Nat. Biotech.*, **34**, 646–651.
22. Hemphill,J., Borchardt,E.K., Brown,K., Asokan,A. and Deiters,A. (2015) Optical Control of CRISPR/Cas9 Gene Editing. *J. Am. Chem. Soc.*, **137**, 5642–5645.
23. Nihongaki,Y., Kawano,F., Nakajima,T. and Sato,M. (2015) Photoactivatable CRISPR-Cas9 for optogenetic genome editing. *Nat. Biotechnol.*, **33**, 755–760.
24. Ohlendorf,R., Vidavski,R.R., Eldar,A., Moffat,K. and Möglich,A. (2012) From dusk till dawn: one-plasmid systems for light-regulated gene expression. *J. Mol. Biol.*, **416**, 534–542.
25. Mathes,T., Vogl,C., Stolz,J. and Hegemann,P. (2009) In vivo generation of flavoproteins with modified cofactors. *J. Mol. Biol.*, **385**, 1511–1518.
26. Leaver-Fay,A., Tyka,M., Lewis,S.M., Lange,O.F., Thompson,J., Jacak,R., Kaufman,K., Renfrew,P.D., Smith,C.A., Sheffler,W. *et al.* (2011) ROSETTA3: an object-oriented software suite for the simulation and design of macromolecules. *Meth. Enzymol.*, **487**, 545–574.
27. Huang,P.-S., Ban,Y.-E.A., Richter,F., Andre,I., Vernon,R., Schief,W.R. and Baker,D. (2011) RosettaRemodel: a generalized framework for flexible backbone protein design. *PLoS ONE*, **6**, e24109.
28. Jinek,M., Jiang,F., Taylor,D.W., Sternberg,S.H., Kaya,E., Ma,E., Anders,C., Hauer,M., Zhou,K., Lin,S. *et al.* (2014) Structures of Cas9 endonucleases reveal RNA-mediated conformational activation. *Science*, **343**, 1247997.
29. Kanwar,M., Wright,R.C., Date,A., Tullman,J. and Ostermeier,M. (2013) Protein switch engineering by domain insertion. *Meth. Enzymol.*, **523**, 369–388.
30. Gibson,D.G., Young,L., Chuang,R.-Y., Venter,J.C., Hutchison,C.A. and Smith,H.O. (2009) Enzymatic assembly of DNA molecules up to several hundred kilobases. *Nat. Methods*, **6**, 343–345.
31. Guntas,G., Hallett,R.A., Zimmerman,S.P., Williams,T., Yumerefendi,H., Bear,J.E. and Kuhlman,B. (2015) Engineering an improved light-induced dimer (iLID) for controlling the localization and activity of signaling proteins. *PNAS*, **112**, 112–117.
32. McClelland,M., Hanish,J., Nelson,M. and Patel,Y. (1988) KGB: a single buffer for all restriction endonucleases. *Nucleic Acids Res.*, **16**, 364.
33. Deltcheva,E., Chylinski,K., Sharma,C.M., Gonzales,K., Chao,Y., Pirzada,Z.A., Eckert,M.R., Vogel,J. and Charpentier,E. (2011) CRISPR RNA maturation by trans-encoded small RNA and host factor RNase III. *Nature*, **471**, 602–607.
34. Fonfara,I., Le Rhun,A., Chylinski,K., Makarova,K.S., Lécrivain,A.-L., Bzdrenga,J., Koonin,E.V. and Charpentier,E. (2013) Phylogeny of Cas9 determines functional exchangeability of dual-RNA and Cas9 among orthologous type II CRISPR-Cas systems. *Nucl. Acids Res.*, **42**, 2577–2590.
35. Nishimasu,H., Ran,F.A., Hsu,P.D., Konermann,S., Shehata,S.I., Dohmae,N., Ishitani,R., Zhang,F. and Nureki,O. (2014) Crystal structure of Cas9 in complex with guide RNA and target DNA. *Cell*, **156**, 935–949.
36. Ohlendorf,R., Schumacher,C.H., Richter,F. and Möglich,A. (2016) Library-aided probing of linker determinants in hybrid photoreceptors. *ACS Synth. Biol.*, doi:10.1021/acssynbio.6b00028.
37. Gasser,C., Taiber,S., Yeh,C.-M., Wittig,C.H., Hegemann,P., Ryu,S., Wunder,F. and Möglich,A. (2014) Engineering of a red-light-activated human cAMP/cGMP-specific phosphodiesterase. *Proc. Natl. Acad. Sci. U.S.A.*, **111**, 8803–8808.
38. Yee,E.F., Diensthuber,R.P., Vaidya,A.T., Borbat,P.P., Engelhard,C., Freed,J.H., Bittl,R., Möglich,A. and Crane,B.R. (2015) Signal in light-oxygen-voltage receptors lacking the adduct-forming cysteine residue. *Nat. Commun.*, **6**, 10079.
39. Heins,R.A., Choi,J.H., Sohka,T. and Ostermeier,M. (2011) In vitro recombination of non-homologous genes can result in gene fusions that confer a switching phenotype to cells. *PLOS ONE*, **6**, e27302.
40. Choi,J.H., San,A. and Ostermeier,M. (2013) Non-allosteric enzyme switches possess larger effector-induced changes in thermodynamic stability than their non-switch analogs. *Protein Sci.*, **22**, 475–485.
41. Sternberg,S.H., Redding,S., Jinek,M., Greene,E.C. and Doudna,J.A. (2014) DNA interrogation by the CRISPR RNA-guided endonuclease Cas9. *Nature*, **507**, 62–67.
42. Chu,B.W., Banaszynski,L.A., Chen,L. and Wandless,T.J. (2008) Recent progress with FKBP-derived destabilizing domains. *Bioorg. Med. Chem. Lett.*, **18**, 5941–5944.
43. Schlapschy,M., Binder,U., Börger,C., Theobald,I., Wachinger,K., Kisling,S., Haller,D. and Skerra,A. (2013) PASylation: a biological alternative to PEGylation for extending the plasma half-life of pharmaceutically active proteins. *Protein Eng. Des. Sel.*, **26**, 489–501.
44. Peters,J.M., Silvis,M.R., Zhao,D., Hawkins,J.S., Gross,C.A. and Qi,L.S. (2015) Bacterial CRISPR: accomplishments and prospects. *Curr. Opin. Microbiol.*, **27**, 121–126.
45. Cleto,S., Jensen,J.V., Wendisch,V.F. and Lu,T.K. (2016) Corynebacterium glutamicum Metabolic Engineering with CRISPR Interference (CRISPRi). *ACS Synth. Biol.*, **5**, 375–385.